AIAA JOURNAL
Vol. 30, No. 12, December 1992

Application of Adaptive Technology to Static Aeroelastic Control of Wing Structures

O. Song,* L. Librescu,† and C. A. Rogers‡
Virginia Polytechnic Institute and State University, Blacksburg, Virginia 24061

The static aeroelastic behavior of adaptive swept-forward wing structures modeled as thin-walled beams and incorporating piezoelectric effects is investigated. Based on the converse piezoelectric effect, the system of piezoelectric layers, embedded or bonded to the wing, yields control of both divergence instability and, in the subcritical speed range, of aeroelastic lift distribution. The numerical illustrations reveal the ability of adaptive technology to control the static aeroelastic response of swept-forward wings and, as a result, to fully exploit the advantages offered by such a wing configuration.

Nomenclature

A_{ij} = stretching rigidities
a_{ij} = rigidity quantities of the beam
B_{ij} = bending-stretching coupling rigidities
B_ω = bimoment
$C_{ij}^{\mathcal{E}}$ = elastic constants (measured under a constant electric field)
C_L = effective lift coefficient
c = wing chord measured perpendicular to the reference axis
D_{ij} = bending rigidities
$\mathcal{E}_k$ = electric field intensity vector, $k = \overline{1,3}$
e = offset between aerodynamic centerline and reference axis
e_{ki} = piezoelectric constants
$F_\omega(s)$ = primary warping function
$h(s)$ = wall thickness of the beam
$\bar{K}_{11}$, $\bar{\bar{K}}_{11}$, $\bar{\bar{\bar{K}}}_{11}$ = modified local stiffness coefficients
K_p = gain factor, $[\theta_x'(L)/\theta_x'(0)]$
L_{zz}, L_{sz} = stress couples
ℓ, m = number of piezoelectric actuator layers and of master structure, respectively
M_x, $-M_y$, M_z = moments in x, y, and z directions, respectively
m_x, $-m_y$, m_z = distributed external moments in x, y, and z directions, respectively
N_{zz}, N_{sz}, N_{nz} = stress resultants
N_{zz}^a = piezoelectrically induced axial stress resultant
p_x, p_y, p_z = distributed loads in x, y, and z directions, respectively
Q_x, Q_y = shear forces in x and y directions, respectively
q_D = divergence dynamic pressure
q_n = dynamic pressure normal to the leading edge
S_{ij}, $\bar{S}_{ij}$, $\bar{\bar{S}}_{ij}$ = various strains
S_j = strain components in contracted notations
(s, z, n) = local coordinate system
T_z = axial force in z direction
$u_0(z)$, $v_0(z)$, $w_0(z)$ = displacement components of the beam axis in x, y, and z directions, respectively
$\underset{\sim}{u}_i$ = specified displacements
α_{eff} = effective angle of attack
γ_{xz}, γ_{yz} = transverse shear strains in x-z and y-z planes, respectively
Θ_0 = rigid angle of attack (measured in planes normal to the leading edge)
$\theta_y(z)$, $\theta_x(z)$, $\Theta(z)$ = rotations of the beam about y, x, and z axes, respectively
Λ = angle of sweep

Subscripts

A, NA = response quantity associated with the adaptive and nonadaptive structures, respectively

Received Sept. 24, 1991; revision received March 25, 1992; accepted for publication April 4, 1992.

*Research Associate, Department of Engineering Science and Mechanics.
†Professor, Department of Engineering Science and Mechanics.
‡Professor and Director, Center for Intelligent Material Systems and Structures.

Introduction

A PROMISING concept that will probably play an important role in the construction of the next generation of supermaneuverable airplanes relies on the incorporation in their design of adaptive materials technology.[1] Recent studies carried out on the experimental fighter F-111 have revealed that adaptive materials technology can provide significant payoffs for mission adaptive wings (MAW) of advanced aircraft (see, e.g., Ref. 2). These higher capabilities accomplished without weight penalties will yield increases in aircraft efficiency, range, speed, maneuverability rate, etc.

The successful development of smart material systems technology could lead to a generation of space vehicles that are lighter, highly maneuverable, and safer to operate in hostile environmental conditions throughout their associated flight envelope without the danger of encountering any aeroelastic instability which would jeopardize their free flight. In contrast to the previous adaptive technologies based on traditional leading- and trailing-edge devices, the variable sweep wing concept (which unavoidably has drag-producing hinges and crevices) or the aeroelastic tailoring technology (which is passive in nature), the adaptive material system concept often involves embedding exotic materials in the structure, thereby facilitating their adaptive function without affecting the external aerodynamic shape.

Despite its exceptional practical importance, it appears that there is a reduced number of published works on the subject of the adaptive technology applied to the control of aeroelastic structural systems. Several results concerning the static and dynamic aeroelasticity of adaptive lifting surfaces can be found in Refs. 3, 4, and 5, respectively, whereas, in Refs. 6 and 7 the induced strain actuation technique is used to control the supersonic flutter of flat panels. For a review paper in this field the reader is referred to Ref. 8.

In the previous work[3,4] the wing structure was modeled as an anisotropic solid beam featuring, in a coupled form, both Bernoulli-Euler bending and St. Venant twist models. In contrast to this modeling of the wing structure, in this paper a more refined yet more realistic model was devised. It consists of a thin/thick-walled closed section cantilevered beam. For

such anisotropic cantilevered beams (of either solid or thin/thick-walled cross section), the warping inhibition induced by the restraint of torsion requires the discard of the St. Venant twist concept. To this end, in the present analysis both the primary and secondary warping restraint effects were incorporated.

Moreover, the transverse shear flexibility characterizing the behavior of advanced composite material systems was taken into consideration. The wing structure featuring these characteristics is considered to be composed of piezoelectric layers (polarized in the thickness direction) superposed on the master structure. The constitutive equations for the composite structure are derived. These equations, used in conjunction with the virtual work principle (extended to a piezoelectric continuum), yield the equations of static aeroelastic equilibrium of adaptive swept-wing structures. The numerical results illustrate in a convincing way the potential role adaptive technology could play to the increase of the divergence instability speed, and within the subcritical speed range, to the decrease of the effective angle of attack throughout the wing span.

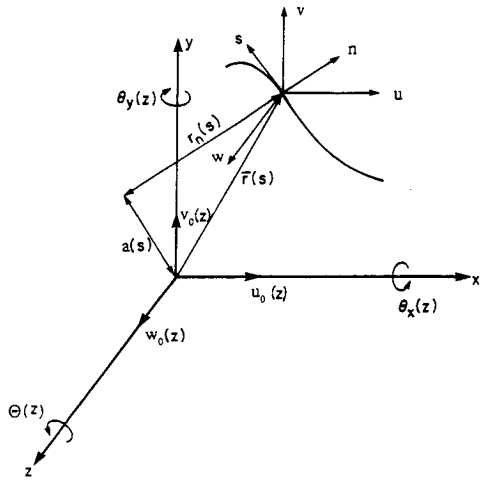

Fig. 1a Coordinate system and kinematic variables.

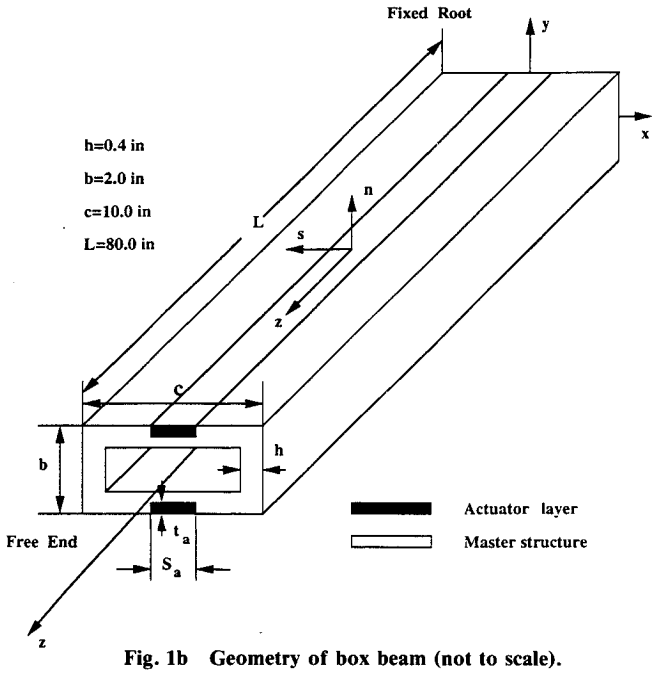

Fig. 1b Geometry of box beam (not to scale).

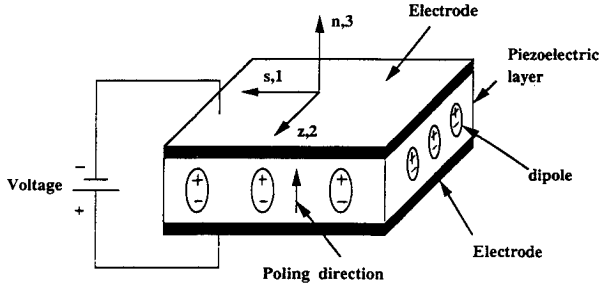

Fig. 1c Actuator layer.

Kinematics

The thin-walled closed section beam model used in the present paper is based on the following kinematic statements[9-12]:

1) The original shape of the cross section of the beam is preserved.

2) The effects due to transverse shear are taken into account. As a result, the considered beam model is also capable of providing results for the case of thick-walled beams and/or when the constituent materials exhibit low rigidities in transverse shear.

3) The rate of twist assumed to vary along the beam axis constitutes a measure of the warping restraint effect. The primary warping displacement is assumed to exhibit the same distribution across the cross section of a beam as the warping function of the St. Venant torsion theory.

4) The secondary warping (whose effect for composite material structures may be comparable to the primary warping) is also incorporated.

Based on the preceding assumptions, the displacement field is expressible as (see Fig. 1a)

$$u(x, y, z) = u_0(z) - y\Theta(z) \tag{1}$$

$$v(x, y, z) = v_0(z) + x\Theta(z) \tag{2}$$

$$w(n, s, z) = w_0(z) + x(s)\theta_y(z) + y(s)\theta_x(z) - F_\omega(s)\Theta'(z) + n\left[\frac{dy}{ds}\theta_y(z) - \frac{dx}{ds}\theta_x(z) - a(s)\Theta'(z)\right] \tag{3}$$

where

$$\theta_y(z) = \gamma_{xz}(z) - u_0'(z) \tag{4}$$

$$\theta_x(z) = \gamma_{yz}(z) - v_0'(z) \tag{5}$$

$$a(s) = -y(s)\frac{dy}{ds} - x(s)\frac{dx}{ds} \tag{6}$$

The expression of the warping function is

$$F_\omega(s) = \int_0^s [r_n(s) - \psi]\, ds \tag{7}$$

where the torsional function ψ is

$$\psi = \frac{\oint_C r_n(s)\frac{ds}{h(s)}}{\oint_C \frac{ds}{h(s)}} \left(\equiv \frac{2A_C}{\beta}\right) \tag{8}$$

and

$$r_n(s) = x(s)\frac{dy}{ds} - y(s)\frac{dx}{ds} \tag{9}$$

As a result, six kinematic variables, $u_0(z)$, $v_0(z)$, $w_0(z)$, $\theta_y(z)$, $\theta_x(z)$, and $\Theta(z)$, representing three rigid-body translations in the x, y, and z directions and three rigid-body rotations about the y, x, and z axis, respectively, are used to define the displacement vector (i.e., the displacement components u, v, and w in the x, y, and z directions, respectively). Here (s, z, n) and (x, y, z) denote the surface and cross-sectional reference coordinate systems, respectively (see Fig. 1a). The quantity $h[\equiv h(s)]$ denotes the wall thickness of the beam (allowed to

vary along the periphery), A_C denotes the cross-sectional area bounded by the midline, β denotes the total length of the contour midline, $\oint_C(\cdot)\,ds$ denotes the integral around the entire periphery C of the beam, and $\int_0^s r_n(s)\,ds[\equiv\Omega(s)]$ in Eq. (7) is referred to as the sectorial area.

Based on the kinematic representations [Eqs. (1-3)], the strain measures assume the following form:

Axial strain:

$$S_{zz}(n,\,s,\,z)=\bar{S}_{zz}(s,z)+n\hat{S}_{zz}(s,\,z) \tag{10}$$

where

$$\bar{S}_{zz}(s,z)=w_0'(z)+\theta_y'(z)x(s)+\theta_x'(z)y(s)-\Theta''(z)F_\omega(s) \tag{11a}$$

and

$$\hat{S}_{zz}(s,z)=\theta_y'(z)\frac{dy}{ds}-\theta_x'(z)\frac{dx}{ds}-\Theta''(z)a(s) \tag{11b}$$

denote the axial strains associated with the primary and secondary warping, respectively.

Membrane shear strain:

$$S_{sz}(s,z)=[\theta_y(z)+u_0'(z)]\frac{dx}{ds}+[\theta_x(z)+v_0'(z)]\frac{dy}{ds}+2\frac{A_C}{\beta}\Theta'(z) \tag{12}$$

Transverse shear strain:

$$S_{nz}(s,\,z)=[\theta_y(z)+u_0'(z)]\frac{dy}{ds}-[\theta_x(z)+v_0'(z)]\frac{dx}{ds} \tag{13}$$

Within the present theory the warping measure is expressible as

$$W_M=\Theta'(z) \tag{14}$$

Here, and in the following developments $(\cdot)'\equiv\partial(\cdot)/\partial z$.

Incorporation of Actuator Patches: Constitutive Equations

The linear constitutive equations for a three-dimensional piezoelectric continuum expressed in the Voigt's contracted indicial notations are (see, e.g., Refs. 13 and 14)

$$\sigma_i=C_{ij}^{\mathcal{E}}S_j-e_{ki}\,\mathcal{E}_k \tag{15a}$$

$$D_k=e_{kj}S_j+\epsilon_{k\ell}^{S}\,\mathcal{E}_\ell \tag{15b}$$

where σ_i and $S_j(i,\,j=\overline{1,6})$ denote the stress and strain components, respectively, where

$$S_j=\begin{cases}S_{pr} & \text{when} \quad p=r,\quad j=1,2,3\\ 2S_{pr} & \text{when} \quad p\neq r,\quad j=4,5,6\end{cases} \tag{16}$$

$C_{ij}^{\mathcal{E}}$ is measured for conditions of constant electric field, and e_{ki} and $\epsilon_{k\ell}^{S}$ are measured under constant strain; and $D_k(k=1,3)$ denotes the electric displacement vector. In Eqs. (15) the summation over repeated indices is implied. Whereas Eq. (15a) describes the converse piezoelectric effect (consisting of the generation of mechanical stress or strain when an electric field is applied), Eq. (15b) describes the direct piezoelectric effect (consisting of generation of an electrical charge in response to a mechanical deformation).

In a piezoelectric adaptive structure, the direct effect is used for distributed sensing, whereas the converse effect is used for active distributed control. Equations (15) are valid for the most general anisotropic case (i.e., for triclinic crystals). In the following we will restrict the generality to the case of a transversely isotropic continuum where the n axis is an axis of rotary symmetry coinciding with the direction of polarization (thickness polarization) (see Fig. 1c). In this case, the piezoelectric continuum is characterized by five independent elastic constants, three independent piezoelectric constants, and two independent dielectric constants. We will assume that $\mathcal{E}_\ell$ is represented in terms of its component $\mathcal{E}_3$ in the n direction only (implying $\mathcal{E}_1=\mathcal{E}_2=0$). Moreover, as result of the uniform voltage distribution, $\mathcal{E}_3$ results as a constant valued quantity.

Equation (16) reveals that a piezoelectric continuum exhibiting anisotropic behavior cannot generate or detect shear stresses/strains by applying or detecting electric fields along the n direction.

In the following developments we will assume that the master structure is composed of m elastic layers exhibiting transversely isotropic behavior, whereas the actuator (superposed on the master structure) is composed of ℓ piezoelectric layers. For the sake of convenience we restrain our considerations to the case where the actuators are distributed over the entire span of the wing. Along the circumferential s and transversal n directions, they are distributed according to the following law[15,16] (see Fig. 2):

$$\begin{aligned}R_{(k)}(n)&=H(n-n_{(k^-)})-H(n-n_{(k^+)})\\ R_{(k)}(s)&=H(s-s_{(k^-)})-H(s-s_{(k^+)})\end{aligned} \tag{17}$$

where H denotes the Heaviside distribution and R is a spatial function. The three-dimensional constitutive equations are

$$\begin{Bmatrix}\sigma_{ss}\\ \sigma_{zz}\\ \sigma_{sz}\end{Bmatrix}_{(k)}=\begin{bmatrix}C_{11} & C_{12} & 0\\ C_{12} & C_{11} & 0\\ 0 & 0 & (C_{11}-C_{12})/2\end{bmatrix}_{(k)}\begin{Bmatrix}S_{ss}\\ S_{zz}\\ S_{sz}\end{Bmatrix}_{(k)}-\begin{Bmatrix}e_{31}^{(k)} & \mathcal{E}_3^{(k)} & R_{(k)}(n) & R_{(k)}(s)\\ e_{31}^{(k)} & \mathcal{E}_3^{(k)} & R_{(k)}(n) & R_{(k)}(s)\\ & & 0 & \end{Bmatrix} \tag{18a}$$

and

$$\begin{Bmatrix}\sigma_{nz}\\ \sigma_{sn}\end{Bmatrix}_{(k)}=\begin{bmatrix}C_{44} & 0\\ 0 & C_{44}\end{bmatrix}_{(k)}\begin{Bmatrix}S_{nz}\\ S_{sn}\end{Bmatrix}_{(k)} \tag{18b}$$

where the index k in brackets affecting a quantity identifies its affiliation to the kth layer. The global beam stress resultants and couples could be obtained through integration of the three-dimensional stress components through the laminate thickness and afterward through the integration of the local stress resultants along the contour of the beam. In the absence of the internal pressure, the hoop stress resultant N_{ss} is negligible compared to the remaining stress resultants (i.e., $N_{ss}\approx 0$) (Ref. 17). In this case, the constitutive equations associated with the local beam stress resultants are defined in terms of the associated strains.

Stress resultants:

$$N_{zz}=\bar{K}_{11}\bar{S}_{zz}+\bar{\bar{K}}_{11}\bar{\bar{S}}_{zz}-N_{zz}^{a} \tag{19a}$$

$$N_{sz}=A_{66}S_{sz} \tag{19b}$$

$$N_{nz}=A_{44}S_{nz} \tag{19c}$$

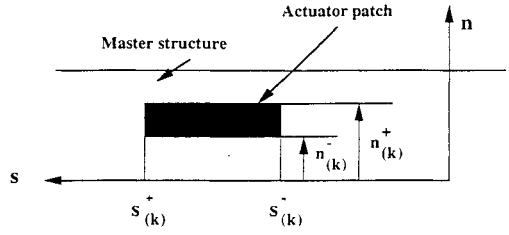

Fig. 2 Actuator patch.

Stress couples:

$$L_{zz} = \bar{\bar{K}}_{11}\bar{S}_{zz} + \bar{\bar{K}}_{11}\bar{\bar{S}}_{11} - L^a_{zz} \tag{20a}$$

$$L_{sz} = B_{66}S_{sz} \tag{20b}$$

In these equations K_{ij} denote the modified local stiffness coefficients, and N^a_{zz} and L^a_{zz} denote the piezoelectrically induced stress resultant and stress couple. Their expressions are displayed in Appendix A.

It should be emphasized that the constitutive equations (19a) and (20a) relate the stress resultants and couples with the strain components and the electric field $\mathcal{E}_3$. The analysis yielding such equations is called "uncoupled" because an approximate solution to the electrostatic problem is postulated, with the result that $\mathcal{E}_3$ is constant.

Equations of Adaptive Thin-Walled Beams

To obtain the equations of equilibrium of an adaptive thin-walled beam and the associated boundary conditions, the static counterpart of Hamilton's variational principle extended to a linear three-dimensional piezoelectric medium[18,19] will be used. It states that

$$\delta\int_\tau(-\mathcal{H} + f_iU_i)\,d\tau + \int_\Omega(\bar{\sigma}_k\delta U_k - \bar{\sigma}\delta\phi)\,d\Omega = 0 \tag{21}$$

where $\mathcal{H}$ denotes the electric enthalpy density, defined as

$$\mathcal{H} = \tfrac{1}{2}C^{\mathcal{E}}_{ij}S_iS_j - e_{ki}S_i - \tfrac{1}{2}\epsilon^S_{k\ell}\mathcal{E}_k\,\mathcal{E}_\ell \tag{22}$$

and where τ and Ω denote the volume and bounding surface of the continuum, respectively; $\bar{\sigma}_k$ denotes the specified surface traction; $\bar{\sigma}$ is the applied surface charge; f_i are the body forces; ϕ is the electric potential; and δ is the variation sign.

After considering in Eq. (21) the displacement components U_i as u_0, v_0, w_0, θ_x, θ_y, and Θ, and S_i as the components defined by Eqs. (10–13), employing $d\tau = dn\,ds\,dz$, and performing the integration across the s and n directions, we can reduce the three-dimensional problem to an equivalent one-dimensional one, in which all the quantities are dependent on the z coordinate only. To this end, the one-dimensional stress resultants and stress couples specific to the theory of thin-walled beams defined in terms of the local beam stress resultants [see Eqs. (19) and (20)] are

$$\begin{aligned}
T_z(z) &\equiv \oint_C N_{zz}\,ds; \quad Q_x(z) = \oint_C\left(N_{sz}\frac{dx}{ds} + N_{zn}\frac{dy}{ds}\right)ds \\
Q_y(z) &= \oint_C\left(N_{sz}\frac{dy}{ds} - N_{zn}\frac{dx}{ds}\right)ds \\
M_x(z) &= \oint_C\left(yN_{zz} - L_{zz}\frac{dx}{ds}\right)ds \\
M_y(z) &= \oint_C\left(xN_{zz} + L_{zz}\frac{dy}{ds}\right)ds \\
M_z(z) &= \oint_C N_{sz}\frac{2A_C}{\beta}\,ds
\end{aligned} \tag{23}$$

and

$$B_\omega(z) = \oint_C [F_\omega(s)N_{zz} + a(s)L_{zz}]\,ds$$

These quantities are referred to as the axial force, the shear forces (in the x and y directions), the moments (in the x, y, and z directions), and the bimoment global quantities. In terms of the one-dimensional stress resultant measures, the equations of equilibrium of the adaptive thin-walled beams are

$$\delta u_0: \quad Q_x' + p_x = 0 \tag{24a}$$

$$\delta v_0: \quad Q_y' + p_y = 0 \tag{24b}$$

$$\delta w_0: \quad T_z' + p_z = 0 \tag{24c}$$

$$\delta\Theta: \quad B_\omega'' + M_z' + m_z + b_\omega' = 0 \tag{24d}$$

$$\delta\theta_x: \quad M_x' - Q_y + m_x = 0 \tag{24e}$$

$$\delta\theta_y: \quad M_y' - Q_x + m_y = 0 \tag{24f}$$

where p_x, p_y, p_z, and m_x, m_y, and m_z are the distributed loads and moments in the x, y, and z directions, respectively; and b_ω is the bimoment of the external loads. By virtue of Eqs. (19a), (20a), (A2), and (23), the stress resultant T_z, the stress couples M_x and M_y as well as the bimoment B_ω could be recast in a form in which the actuator effect appears explicitly:

$$\begin{aligned}
T_z &= \tilde{T}_z - \tilde{\tilde{T}}_z; \qquad M_x = \tilde{M}_x - \tilde{\tilde{M}}_x \\
M_y &= \tilde{M}_y - \tilde{\tilde{M}}_y; \qquad B_\omega = \tilde{B}_\omega - \tilde{\tilde{B}}_\omega
\end{aligned} \tag{25}$$

where the quantities affected by a single overtilde and double overtildes identify the pure mechanical and piezoelectric contributions to the indicated quantities, respectively. Representation of stress resultants and stress couples in terms of displacement quantities u_0, v_0, w_0, θ_x, θ_y, and Θ, and their replacement in Eqs. (24b), (24d), and (24e), together with consideration in Eqs. (24b) and (24d) (associated with the plunging and torsional displacements) of the loads of aerodynamic nature expressed in conjunction with the strip theory aerodynamics, i.e.,

$$p_y = q_nca_0(\Theta_0 + \Theta - v_0'\tan\Lambda) - NW/2L \tag{26a}$$

$$m_z = q_nca_0e(\Theta_0 + \Theta - v_0'\tan\Lambda) + q_nc^2C_{MAC} - NWd/2L \tag{26b}$$

yields the static aeroelastic governing equations in terms of the basic unknowns of the problem. In Eqs. (26), $q_n[\equiv(\rho/2)U_n^2]$ denotes the dynamic pressure normal to the leading edge of the swept wing; a_0 denotes the "corrected lift" curve slope coefficient; Λ is considered positive for swept-back wings; C_{MAC} is the wing section pitching moment coefficient; $W/2L$ denotes the airplane weight per unit length of wing span; N represents the load factor normal to the wing surface; and d denotes the distance between the lines of centers of mass to the elastic axis.

From the virtual work principle the following boundary conditions result. At the clamped edge ($z = 0$),

$$u_0 = \underset{\sim}{u}_0 \tag{27a}$$

$$v_0 = \underset{\sim}{v}_0 \tag{27b}$$

$$w_0 = \underset{\sim}{w}_0 \tag{27c}$$

$$\theta_x = \underset{\sim}{\theta}_x \tag{27d}$$

$$\theta_y = \underset{\sim}{\theta}_y \tag{27e}$$

$$\Theta = \underset{\sim}{\Theta} \tag{27f}$$

$$\Theta' = \underset{\sim}{\Theta}' \tag{27g}$$

and at the free edge ($z = L$),

$$Q_x = \underset{\sim}{Q}_x \tag{28a}$$

$$Q_y = \underset{\sim}{Q}_y \tag{28b}$$

$$T_z = \underset{\sim}{T}_z \tag{28c}$$

$$M_y = \underset{\sim}{M}_y \tag{28d}$$

$$\underline{M_x = \underset{\sim}{M}_x} \tag{28e}$$

$$\underline{M_z + B'_\omega = \underset{\sim}{M}_z} \tag{28f}$$

$$\underline{B_\omega = \underset{\sim}{B}_\omega} \tag{28g}$$

where the quantities affected by an undertilde are the prescribed ones. It could be verified that, consistent with the number of seven boundary conditions at each edge, a 14th-order governing equation system is obtained.

In the case of the general anisotropy of the layer materials (i.e., of the master structure, of the actuators, or of both), the system of governing equations appears in a complete coupled form. However, within the anisotropy considered here, the governing equations obtainable from Eqs. (24b), (24d), and (24e) (which are involved in our study) appear decoupled from the remaining ones [resulting from the equations of equilibrium (24a), (24c), and (24f)]. Associated with the former set of three governing equations expressed in terms of the unknown functions v_0, θ_x, and Θ (of the eighth order), the associated four boundary conditions are the ones underlined in Eqs. (27) and (28). Considering the case of homogeneous boundary conditions and recognizing that the stress resultants and moments as they enter the homogeneous boundary conditions also contain piezoelectric effects [see Eqs. (19a), (20a), (A2), and (25)], the boundary conditions at $z = L$ expressed in terms of displacement quantities are

$$a_{33}\theta'_x(L) = \tilde{\tilde{M}}_x \tag{29a}$$

$$a_{55}(v'_0 + \theta_x) = 0 \tag{29a}$$

$$a_{66}\Theta''' + a_{77}\Theta' = 0 \tag{29c}$$

$$a_{66}\Theta'' = \tilde{\tilde{B}}_\omega \tag{29d}$$

whereas at $z = 0$ the boundary conditions are

$$v_0 = \theta_x = \Theta = \Theta' = 0 \tag{30}$$

In Eqs. (29) the coefficients a_{33}, a_{55}, a_{66}, and a_{77} are rigidity quantities, and $\tilde{\tilde{M}}_x$ and $\tilde{\tilde{B}}_\omega$ are the piezoelectrically induced moment and bimoment, respectively. Their expression is displayed in Appendix B.

In light of the actuator configuration, it should be noted that $\tilde{\tilde{M}}_x$ and $\tilde{\tilde{B}}_\omega$ as expressed by Eq. (B2) are independent on the z coordinate. As a result, their contribution in the governing equations is immaterial, whereas in the boundary conditions they intervene as nonhomogeneous terms. Their effects on the divergence instability and distribution of aeroelastic aerodynamic loads will be further investigated.

At this point it should be emphasized that, in contrast to the divergence instability case, which is treated as an eigenvalue problem, the static response implying determination of Θ and v'_0 requires the solution of the governing system of equations. Recognizing that

$$N = \frac{2cq_n a_0}{W}\int_0^L (\Theta_0 + \Theta - v'_0 \tan\Lambda)\, dz \tag{31}$$

Eqs. (24b), (24d), and (24e), in conjunction with Eqs. (26) and (31), constitute an integro-differential equation system. For the case of Θ_0 specified, to reduce the solution of the problem to that of a differential equation system, an iteration process has to be used. Consistent with this procedure, N in Eqs. (26a) and (26b) is assimilated to a constant that has to be evaluated in an iterative way.

Numerical Examples

The adaptive wing is modeled as a symmetric composite box beam (Fig. 1b). The piezoceramic actuator layers (selected to be of PZT-4 ceramic) are located on the upper and bottom surfaces of the master structure only. The geometrical characteristics are displayed in Figs. 1b and 1c. The constants characterizing the PZT-4 piezoceramic used in this paper can be found in Ref. 20.

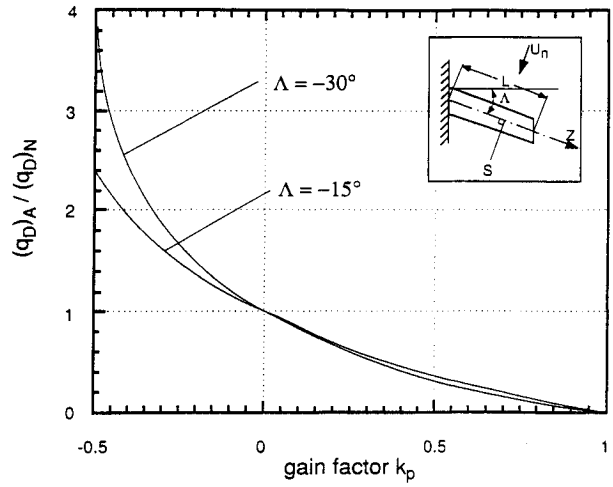

Fig. 3 Variation of $(q_D)_A/(q_D)_{NA}$ vs feedback gain for two sweep-angle wing configurations.

For convenience we assume that the master structure is composed of a transversely isotropic material whose elastic characteristics are identical to those of piezoceramic actuator layers. The adaptive nature of the swept wing is introduced by requiring the applied electric field $\mathcal{E}_3$ to be proportional to the bending moment at the wing root $\tilde{M}_x(0)$, which yields

$$\mathcal{E}_3 = c_1\tilde{M}_x(0) \tag{32}$$

or, in terms of displacement quantities,

$$\mathcal{E}_3 = c_1 a_{33}\theta'_x(0) \tag{33}$$

On the other hand, the piezoelectrically induced moment $\tilde{\tilde{M}}_x$ is given by

$$\tilde{\tilde{M}}_x = c_2\mathcal{E}_3 \tag{34}$$

which, by virtue of Eq. (34), yields

$$\tilde{\tilde{M}}_x = c_1 c_2 a_{33}\theta'_x(0) \tag{35}$$

However, in light of Eq. (29a) we may express Eq. (34) as

$$\theta'_x(L) = K_p\theta'_x(0) \tag{36}$$

where K_p is the feedback gain. This control law [Eq. (36)] is a statement of the proportionality of the control bending moment at the wing tip (induced piezoelectrically) with the mechanical one at the wing root (which increases with the increase of the aircraft speed). Equations (24b), (24d), and (24e) (expressed in terms of displacements), coupled with the control law [Eq. (36)], were solved in conjunction with boundary conditions (27b), (27d), (27g), (27f), and (29) to determine either the eigenvalues (i.e., the divergence speed) or the static response characteristics (implying prior determination of Θ and v'_0). Thus, the effective angle of attack

$$\alpha_{\text{eff}} = \Theta_0 + \Theta - v'_0 \tan\Lambda \tag{37}$$

and, consequently, the effective lift coefficient distribution,

$$C_L = \frac{dC_L}{d\alpha}(\Theta_0 + \Theta - v'_0 \tan\Lambda) \tag{38}$$

along the wing span can be determined. Needless to say, the goal of the control is to maximize the divergence speed and to

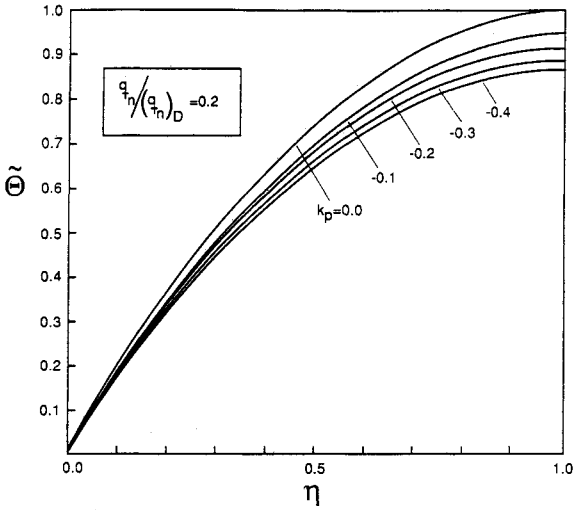

Fig. 4 Variation of $\tilde{\Theta}$ vs η for various K_p, $[q_n/(q_n)_D = 0.2, N = 0]$.

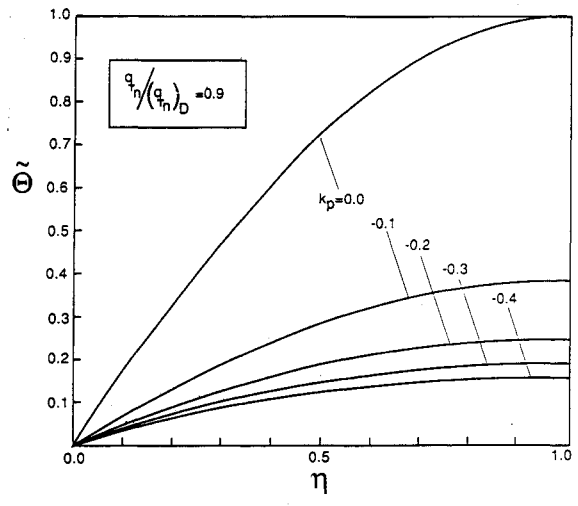

Fig. 5 Variation of $\tilde{\Theta}$ vs η for various K_p, $[q_n/(q_n)_D = 0.9, N = 0]$.

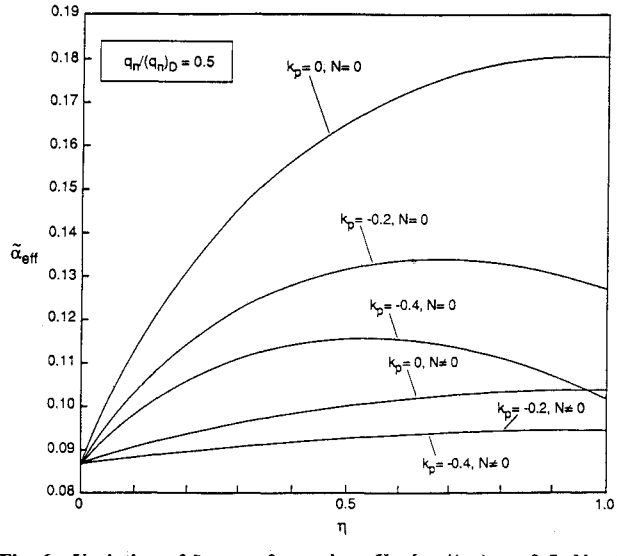

Fig. 6 Variation of $\tilde{\alpha}_{eff}$ vs η for various K_p, $[q_n/(q_n)_D = 0.5, N = 0]$.

attenuate the lift distribution, especially when a swept-forward-wing aircraft is involved.

In Fig. 3, the variation of $\tilde{q}_D[\equiv (q_D)_A/(q_D)_{NA}]$ vs the feedback gain for two sweep angle configuration wings is depicted, where $(q_D)_A$ and $(q_D)_{NA}$ denote the divergence speed of the adaptive wing and its nonadaptive counterpart, respectively. However, in the remainder, the analysis is confined to the case $\Lambda = -30$ deg only. The similarity of the trend of variation of $\tilde{q}_D$ vs K_p as resulting from this figure with the one obtained within the solid beam model[3] is noteworthy.

Figure 4 displays the variation of $\tilde{\Theta}[\equiv \Theta_A(\eta)/\Theta_{NA}(1)]$ vs $\eta(\equiv z/L)$ for various values of the K_p and $N = 0$, where $\Theta_A(\eta)$ and $\Theta_{NA}(1)$ denote the torsional angles experienced by the

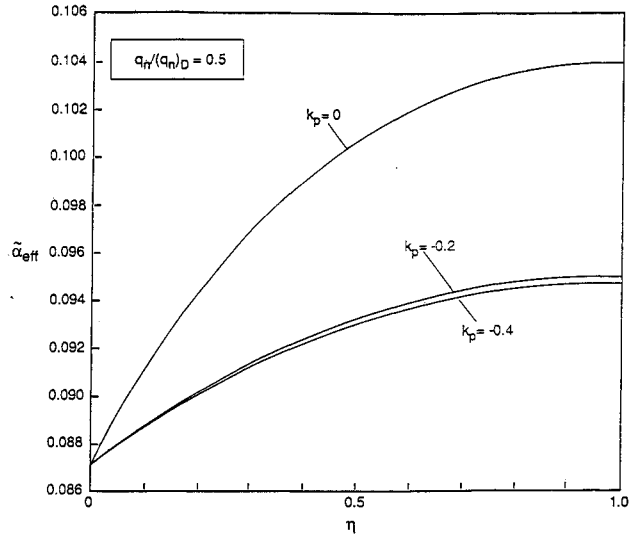

Fig. 7 Variation of $\tilde{\alpha}_{eff}$ vs η for various K_p, $[q_n/(q_n)_D = 0.5, N \neq 0]$.

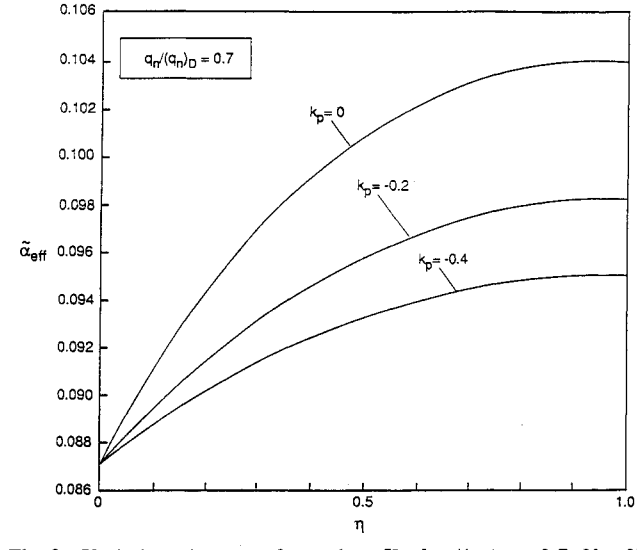

Fig. 8 Variation of $\tilde{\alpha}_{eff}$ vs η for various K_p, $[q_n/(q_n)_D = 0.7, N \neq 0]$.

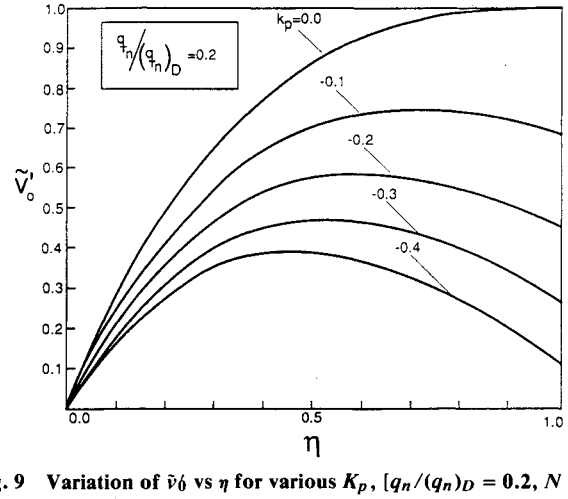

Fig. 9 Variation of $\tilde{v}_0'$ vs η for various K_p, $[q_n/(q_n)_D = 0.2, N = 0]$.

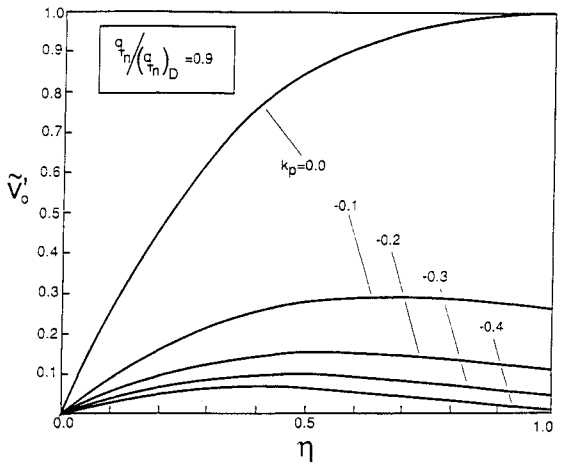

Fig. 10 Variation of $\tilde{v}_0'$ vs η for various K_p, $[q_n/(q_n)_D = 0.9, N = 0]$.

adaptive wing and its nonadaptive counterpart (at $\eta = 1$), respectively. In the determination of this plot, the aircraft speed was considered to be $q_n = 0.2(q_n)_D$, where $(q_n)_D$ is the divergence speed of the nonadaptive wing.

In Fig. 5 the same variation is displayed but for the case where $q_n = 0.9(q_n)_D$.

In Figs. 6 and 7 the variations of $\tilde{\alpha}_{\text{eff}}$ $[\equiv (\alpha_{\text{eff}})_A/(\alpha_{\text{eff}})_{NA}]$ for $N = 0$ and $N \neq 0$ vs η are depicted. Here $q_n = 0.5(q_n)_D$, whereas in Fig. 8 the same variation, but for the case $q_n = 0.7(q_n)_D$ for $N \neq 0$, is displayed. In Figs. 9 and 10, the variation of $\tilde{v}_0'[\equiv (v_0')_A/(v_0'(1))_{NA}]$ vs η for various values of the feedback gain and for two values of q_n, namely, $q_n = 0.2(q_n)_D$ and $q_n = 0.9(q_n)_D$, is displayed.

Whereas Fig. 3 reveals that such an adaptive wing could experience an important increase in divergence speed (namely, four times or more than the one corresponding to its nonadaptive counterpart), the remaining figures reveal the power of the adaptive control technique also in the subcritical speed range. Figures 4–9 reveal that the adaptive forward-swept wing can control the increase of its elastic deformations, i.e., of both Θ and $\tilde{v}_0'$ in the subcritical speed range, so that strong attenuation of the effective angle of attack and of the lift coefficient can be achieved.

Although in the present analysis the transverse shear flexibility effects were incorporated, because of the low anisotropy featured by the PZT-4 piezoceramic materials, its role, compared to the case when this effect is discarded, is very limited. However, this effect could become very significant if materials exhibiting higher transverse shear flexibilities are considered. It should be mentioned that, in the determination of the divergence speed and of the static aeroelastic response, an exact approach based on Laplace transform technique devised in Refs. 21–23 and extended afterward in Refs. 9–11 was used.

It should also be pointed out that in this analysis the issue associated with actuators saturation was not addressed.

Conclusions

A study of the static aeroelastic behavior of adaptive swept-forward-wing structure was accomplished. The structure was modeled as a thin-walled beam, with a theory that incorporates a number of nonclassical effects, such as material anisotropy and heterogeneity, the warping restraint (primary and secondary), transverse shear, as well as the presence of piezoelectric actuator layers. The obtained results reveal the great potential offered by such an adaptive wing to control the divergence instability and the aeroelastic lift distribution on a forward swept wing by mitigating the wash-in effect. They also reveal that the attenuation of elastic deformations becomes more prominent and, consequently, the wing adaptiveness becomes more efficient as the speed increases toward the divergence speed. This yields the conclusion that, by adaptively eliminating the shortcomings of aeroelastic nature, the full advantages offered by the swept-forward-wing configuration airplane could be exploited.

Appendix A

Expression of the modified local stiffness coefficients intervening in Eqs. (19) and (20):

$$\bar{K}_{11} = A_{11} - \frac{A_{12}^2}{A_{11}};\quad \bar{\bar{K}}_{11} = B_{11} - \frac{B_{12}A_{12}}{A_{11}};\quad \bar{\bar{\bar{K}}}_{11} = D_{11} - \frac{B_{12}^2}{A_{11}} \tag{A1}$$

$$N_{zz}^a = \left(1 - \frac{A_{12}}{A_{11}}\right)\sum_{k=1}^{\ell} \mathcal{E}_3^{(k)}(n_{(k+)} - n_{(k-)})e_{31}^{(k)}R_{(k)}(s, z) \tag{A2}$$

$$L_{zz}^a = \sum_{k=1}^{\ell} \mathcal{E}_3^{(k)}e_{31}^{(k)}R_{(k)}(s, z)(n_{(k+)} - n_{(k-)})\left[\frac{1}{2}(n_{(k+)} + n_{(k-)}) - \frac{B_{12}}{A_{11}}\right]$$

whereas

$$A_{ij} = \sum_{k=1}^{m+\ell} C_{ij}^{(k)}(n_{(k)} - n_{(k-1)})$$

$$B_{ij} = \frac{1}{2}\sum_{k=1}^{m+\ell} C_{ij}^{(k)}(n_{(k)}^2 - n_{(k-1)}^2) \tag{A3}$$

$$D_{ij} = \frac{1}{3}\sum_{k=1}^{m+\ell} C_{ij}^{(k)}(n_{(k)}^3 - n_{(k-1)}^3)$$

define the stretching, bending-stretching, and bending stiffness quantities, respectively. In Eqs. (A2), for the sake of brevity the following notation was introduced:

$$R_{(k)}(s, z) \equiv R_{(k)}(s)R_{(k)}(z) \tag{A4}$$

Appendix B

Expression of rigidity quantities intervening in Eqs. (29):

$$a_{33} = \oint_C \left[\bar{K}_{11}y^2 + \bar{\bar{K}}_{11}\left(\frac{dx}{ds}\right)^2\right] ds$$

$$a_{55} = \oint_C \left[A_{66}\left(\frac{dy}{ds}\right)^2 + A_{44}\left(\frac{dx}{ds}\right)^2\right] ds$$

$$a_{66} = -\oint_C [\bar{K}_{11}F_\omega^2 + \bar{\bar{K}}_{11}a^2]\, ds \tag{B1}$$

$$a_{77} = \oint_C A_{66}\left(\frac{2A_C}{\beta}\right)^2 ds$$

$$\tilde{\bar{M}}_x = \oint_C \sum_{k=1}^{\ell} \mathcal{E}_3^{(k)}(n_{(k+)} - n_{(k-)})e_{31}^{(k)}R_{(k)}(s, z)\left[y\left(1 - \frac{A_{12}}{A_{11}}\right) + \frac{dx}{ds}\frac{B_{12}}{A_{11}}\right] ds - \frac{1}{2}\oint_C \left[\frac{dx}{ds}\sum_{k=1}^{\ell} \mathcal{E}_3^{(k)}(n_{(k+)}^2 - n_{(k-)}^2)e_{31}^{(k)}R_{(k)}(s, z)\right] ds \tag{B2}$$

$$\tilde{\bar{B}}_\omega = \oint_C \sum_{k=1}^{\ell} \mathcal{E}_3^{(k)}(n_{(k+)} - n_{(k-)})e_{31}^{(k)}R_{(k)}(s, z)\left[F_\omega\left(1 - \frac{A_{12}}{A_{11}}\right) - a(s)\frac{B_{12}}{A_{11}}\right] ds + \frac{1}{2}\oint_C \left[a(s)\sum_{k=1}^{\ell} \mathcal{E}_3^{(k)}(n_{(k+)}^2 - n_{(k-)}^2)e_{31}^{(k)}R_{(k)}(s,z)\right] ds$$

When the actuators are symmetrically located across the thickness of the beam, the terms indicated by a double underline in Eqs. (B2) vanish.

References

[1]Rogers, C. A., "An Introduction to Intelligent Material Systems and Structures," *Intelligent Structures*, edited by K. P. Chong,

S. C. Liu, and J. C. Li, Elsevier Applied Science, London, 1990, pp. 3–41.

[2]DeCamp, R. H., and Hardy, R., "Mission Adaptive Wing Advanced Research Concepts," AIAA Paper 82-2088, April 1984.

[3]Ehlers, S. M., and Weisshaar, T. A., "Static Aeroelastic Behavior of an Adaptive Laminated Piezoelectric Composite Wing," *Proceeding of the AIAA/ASME/ASCE/AHS/ASC 31st Structures, Structural Dynamics, and Materials Conference,* Long Beach, CA, April 2–4, 1990.

[4]Lazarus, K. B., Crawley, E. F., and Bohlmann, J. D., "Static Aeroelastic Control Using Strain Actuated Adaptive Structures," *Journal of Intelligent Material Systems and Structures,* Vol. 2, No. 3, July 1991, pp. 386–410.

[5]Lazarus, K. B., Crawley, E. F., and Lin, C. Y., "Fundamental Mechanisms of Aeroelastic Control With Control Surface and Strain Attenuation," *Proceedings of the AIAA/ASME/ASCE/AHS/ASC 32nd Structures, Structural Dynamics, and Materials Conference,* Baltimore, MD, April 1991, AIAA Paper 91-0985-CP.

[6]Scott, R. C., and Weisshaar, T. A., "Controlling Panel Flutter Using Adaptive Materials," *Proceedings of the AIAA/ASME/ASCE/AHS/ASC 32nd Structures, Structural Dynamics, and Materials Conference,* Baltimore, MD, April 8–10, 1991, AIAA Paper 91-1067-CP.

[7]Hajela, P., and Glowasky, R., "Application of Piezoelectric Elements in Supersonic Panel Flutter Suppression," AIAA Paper 91-3191, Sept. 1991.

[8]Weisshaar, T. A., and Ehlers, S. M., "Adaptive Aeroelastic Composite Wings—Control and Optimization Issues," US-SSSR Conference on Composite Materials, Albany, NY, 1991 (preprint).

[9]Librescu, L., and Song, O., "Static Aeroelastic Tailoring of Composite Aircraft Wings Modelled as Thin-Walled Beam Structures," *Achievements in Composites in Japan and the United States,* edited by A. Kobayashi, Fifth Japan-U.S. Conference on Composite Materials, Tokyo, Japan, June 24–27, 1990, pp. 141–149.

[10]Librescu, L., and Song, O., "Behavior of Thin-Walled Beams Made of Advanced Composite Materials and Incorporating Non-Classical Effects," *Mechanics Pan American Applied Mechanics Review,* Vol. 44, edited by R. A. Kitte and D. T. Mook, No. 11, Pt. 2, Nov. 1991, pp. 174–180.

[11]Song, O., and Librescu, L., "Free Vibration and Aeroelastic Divergence of Aircraft Wings Modelled as Composite Thin-Walled Beams," *Proceedings of the AIAA/ASME/ASCE/AHS/ASC 32nd Structures, Structural Dynamics and Materials, Conference,* Baltimore, MD, April 8–10, 1991, AIAA Paper 91-1187.

[12]Rehfield, L. W., Atilgan, A. R., and Hodges, D. H., "Nonclassical Behavior of Thin-Walled Composite Beams," *Journal of the American Helicopter Society,* Vol. 35, No. 2, April 1990, pp. 42–50.

[13]Mason, W. P., *Crystal Physics of Interaction Processes,* Academic Press, New York, 1966.

[14]"IEEE Standard on Piezoelectricity," IEEE Std. 176–1978, Institute of Electrical and Electronics Engineers, New York, 1978.

[15]Wang, B.-T., and Rogers, C. A., "Laminate Plate Theory for Spatially Distributed Induced Strain Actuators," *Journal of Composite Materials,* Vol. 25, No. 4, April 1991, pp. 433–452.

[16]Wang, B.-T., and Rogers, C. A., "Modeling of Finite-Length and Spatially-Distributed Induced Strain Actuators for Laminate Beams and Plates," *Journal of Intelligent Materials Systems and Structures,* Vol. 2, No. 1, Jan. 1991, pp. 38–58.

[17]Rehfield, L. W., "Design Analysis Methodology for Composite Rotor Blades," *Proceedings of the Seventh DOD/NASA Conference on Fibrous Composites in Structural Design,* Denver, CO, AFWAL-TR-85-3094, June 1985, pp. v(a)-1)–v(a)15).

[18]Tiersten, H. F., *Linear Piezoelectric Plate Vibrations,* Plenum Press, New York, 1969.

[19]Lee, P. C. Y., and Haynes, D. W., "Piezoelectric Crystals and Electro-Elasticity," *R. D. Mindlin and Applied Mechanics,* edited by G. Hermann, Pergamon Press, New York, 1977, pp. 227–253.

[20]Berlincourt, D. A., Curran, D. R., and Jaffe, H., "Piezoelectric and Piezomagnetic Materials and Their Function in Transducers," *Physical Acoustics—Principles and Methods,* Vol. 1, edited by W. P. Mason, Pt. A, Academic Press, New York, 1964, pp. 169–270.

[21]Librescu, L., and Thangjitham, S., "The Static Aeroelastic Behavior of Sweptforward Composite Wing Structures Taking into Account Their Warping Restraint Effect," *Proceedings of the Fourth Japan–U.S. Conference on Composite Materials,* Technomic, Lancaster, PA, 1988, pp. 914–922.

[22]Librescu, L., and Thangjitham, S., "The Warping Restraint Effect in the Critical and Subcritical Static Aeroelastic Behavior of Swept-Forward Composite Wing Structures," *1989 Society of Automotive Engineers General Aviation Aircraft Meeting and Exposition,* Century II, Wichita, KS, April 11–13, 1989; also Paper 891056.

[23]Librescu, L., and Thangjitham, S., "Analytical Studies on Static Aeroelastic Behavior of Forward-Swept Composite Wing Structures," *Journal of Aircraft,* Vol. 28, No. 2, 1991, pp. 151–157.